JOURNAL OF GEOPHYSICAL RESEARCH, VOL. 105, NO. C8, PAGES 19,745–19,762, AUGUST 15, 2000

Laboratory study of wave bottom interaction in the bar formation on an erodible sloping bed

C. Dulou and M. Belzons
Institut Universitaire des Systèmes Thermiques Industriels, Université de Provence
Marseille, France

V. Rey
Laboratoire des Sondages Electromagnétiques de l'Environnement Terrestre, Université de Toulon
La Garde, France

Abstract. The interaction between partially standing or almost progressive surface gravity waves and erodible beds is investigated in a small wave tank under nonbreaking wave conditions. The bed is initially flat and gently sloping, and the incident weakly nonlinear wave is either a regular wave (similar to a Stokes wave), or a regular wave superimposed on a free wave generated by the wave maker (bichromatic or bimodal wave). Accurate measurements of both the bed profile and the wave envelope are performed, showing a permanent coupled evolution of the wave field and of the bed shape. Sandbar formation is observed in the ultimate bed profile which reproduces the spatial modulations of the envelope of the first harmonic of the wave (e.g., the fundamental component). In the case of a pure regular wave, the interbar spacing is equal to half the local surface wavelength which corresponds to a first-order Bragg resonance with the local wavenumber of the first harmonic satisfying the dispersion relation for small waves. In the case of a bimodal wave the preceding case is perturbed by a free wave of the same frequency and similar amplitude as the second harmonic of the regular wave. Then, nonlinear interactions between the first harmonic and the free wave occur, leading to sum and difference frequencies. The difference interaction modifies the amplitude and spatial modulation of the first harmonic. The Bragg resonance mechanism based on the first harmonic in the bar formation is then modified. However, in this case, the bed profile is also the replica of the envelope of the first harmonic of the wave: the perturbation induced in the first harmonic is also present in the bed shape. For partially standing bimodal waves, the Fourier analysis of the bed profile shows a second spatial modulation with the local wavenumber of the free wave. For almost progressive bimodal waves, a third modulation is found with the local wavenumber of the observed beating between the free wave and the second harmonic component of the wave.

These modulations of the envelope of the first harmonic are recovered analytically through a partially standing bimodal wave modeling. This study confirms that the bar formation under nonbreaking wave conditions is controlled by the envelope of the first harmonic of the wave even if perturbed by a free wave.

1. Introduction

A wave propagating in a nonhomogeneous medium undergoes many partial reflections and transmissions. The wave is thus the result of a multiple interference process between all the partial waves resulting from individual scatterers. When the scatterers are periodically placed in the medium, a strong backward reflection may be observed as a result of a phase matching between individual waves. The amplitude of the reflection is observed to increase with the number of scatterers. This phenomenon is well known in solid-state physics and referred to as Bragg reflection. It may be observed in a wide variety of scientific fields where the propagating wave encounters some periodicity. In the case of a wave of wavenumber k propagating in a one-dimensional periodic medium of wavenumber K, the phase matching is obtained when $k = K/2$, that is, when the wavelength of the wave is twice the wavelength of the medium. More generally, the interaction

Copyright 2000 by the American Geophysical Union.

Paper number 2000JC900082.
0148-0227/00/2000JC900082$09.00

of an incident wave of wavenumber k_n with a periodic medium of wavenumber K will give rise to Bragg resonance of nth order if the Bragg condition $k_n = nK/2$ is satisfied (n integer).

The Bragg reflection is also of importance in physical oceanography and in coastal engineering, where waves scattering by fixed obstacles or by changes in seabed topography are observed. In this context, the dynamic evolution of sandy beds toward almost sinusoidal topographies, under partially standing nonlinear waves, is of particular interest.

Patches of shore-parallel bars are often observed over gently sloping bottoms outside the surf zone, with heights of the order of 1 m and spacing in the range of 10 to 100 m, increasing with water depth. The issue is the role of the Bragg mechanism in the natural situation. The reflection of waves by bottom undulations was first proposed by *Ursell* [1947] and later identified by *Davies* [1982]. More recently, it was extensively studied, both theoretically and experimentally, for solid modulated beds of constant mean water depth [*Davies and Heathershaw,* 1983; *Guazzelli et al.,* 1992; *Kirby,* 1986; *Kirby,* 1989; *Mei,* 1985; *Nayfeh and Hawwa,* 1994; *O'Hare and Davies,* 1990; *Rey et al.,* 1995; *Rey et al.,* 1996] and over sloping mean depth [*Mei,* 1985; *Mei et al.,* 1988; *Rey and Fraunié,* 1997]. The bar formation under wave action has been extensively investigated in both the field [*Dette,* 1980; *Saylor and Hands,* 1970; *Short,* 1975] and the laboratory [*O'Hare and Davies,* 1990; *Rey et al.,* 1995; *Brooke-Benjamin et al.,* 1987; *Scott,* 1954] for bottoms of constant mean water depth.

A possible model of sedimentary bar formation under the action of a weakly nonlinear surface wave is based on a boundary layer model of the wave-bed interaction [*O'Hare and Davies,* 1993]. The sediment is shed from small-scale ripples into suspension in the near-bed region, considered as a turbulent boundary layer. This boundary layer is developed under the forcing of an external linear potential flow, representing the first harmonic of the surface wave. The subsequent redistribution of sediment is dominated by the envelope of the first harmonic of the wave whose eventual spatial modulations are finally reproduced in the bottom profile. As the partially standing wave field, produced by partial reflection of an incident regular wave, of wavenumber k has an envelope of wavenumber $2k$, the bed erosion under the action of such a wave is expected to produce a bar system of wavenumber $K_B = 2k$, that is, of interbar spacing of half the wavelength of the incident surface wave. Finally, the mechanism of the bar formation is controlled by the Bragg resonance condition and the development of such a bar system reinforces the rate of standing waves through resonant Bragg reflection of the eroding wave.

The case of a bed load dominated sediment transport has been also studied theoretically [*Yu and Mei,* 2000a]. In the resulting model of bar formation, the prominent role of the Bragg mechanism is again evidenced.

In the particular case of surface gravity waves, the wave-sandbed interaction is a physical example in which the propagation of a nonlinear wave is governed by an evolving bottom condition through wave-bed evolution. The bar formation may be then considered as a dynamically stable solution. Moreover, nonlinear wave-wave interactions observed in shallow water may give rise to perturbations of the envelope of the first harmonic of the wave. Since the bed adaptation is thought to depend on the spatial modulations of the envelope of the first harmonic through Bragg's resonance mechanism, we can expect to deduce from it some of the wave properties, including the nonlinear wave-wave interactions due to the sandbed evolution.

This issue has motivated this laboratory study on the formation of bars under the action of a partially standing wave field on an initially flat sloping erodible bed [*Dulou et al.,* 1998] (where the wave modulations depend on the water depth). This study has been carried out with weakly nonlinear monochromatic waves of frequency f_0 (pure regular wave). However, this wave was superimposed (depending on the bottom configuration) on an unwanted free wave of small amplitude and having the frequency $2f_0$. In this last case, the nonlinear interaction between the first harmonic and the free wave is expected to produce terms of first harmonic frequency and then a small perturbation of the envelope of the first harmonic. This perturbation of the first harmonic of the wave is an example of the energy transfer toward low frequencies observed in nature, leading to infragravity waves [*Ruessink,* 1998; *Norheim et al.,* 1998; *Elgar et al.,* 1997] and participating in the bar formation. However, in the field the wave-wave interactions may be highly nonlinear and then the boundary layer model of bar formation is irrelevant. The aim of this study is to simplify the natural situation (multifrequency spectrum, strong nonlinearities) by addressing the effect of weakly nonlinear interaction in a bimodal wave on the bar formation under nonbreaking wave conditions.

In section 2 the experimental setup is described; in section 3 the results for various wave heights, including nonlinear effects and beach reflection effects, are presented. Finally, these results are discussed in section 4, where a bimodal wave model is proposed, the role of the envelope of the first harmonic of the wave in the bar formation is emphasized, and the reflecting power of the bars is discussed.

2. Experimental Techniques

2.1. Wave Generation

The experiments were carried out in a glass-walled wave tank of 4.7 m long and 0.39 m wide with a maximum water depth of 0.15 m (Figure 1). At one end of the tank a paddle wave maker produced the gravity wave which was either reflected or absorbed by a sloping beach located at the other end. In order to examine its response to the wave field, a layer of artificial noncohesive sand (glass spheres of density $\rho_S = 2.7$ g cm^{-3},

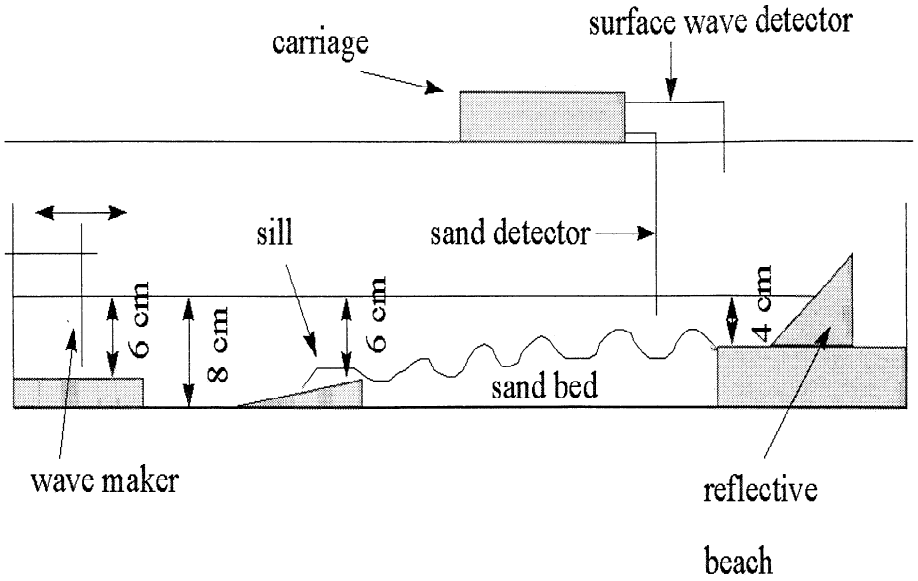

Figure 1. Sketch of the wave tank.

median diameter $D = 0.0080$ cm) was placed in a region extending from 1.2 m downstream of the wave maker to 0.26 m upstream of the toe of the beach slope. The initial sandbed profile was a sloping plane extending over a length L_{sb} (typically 2 m), from a water depth $h_0 = 8$ cm, to a water depth $h_1 = 4$ cm. The bed was continued downstream with a horizontal solid plane of length of 0.26 m and then by the beach.

The vertical wave maker is powered by a linear motor fed through an arbitrary waveform generator (Fluke and Philips PM 5150). It can produce both regular and irregular waves. In the experiments the generated waves were regular, of frequency f_0 selected in the range 1 to 2 Hz (with an accuracy of 0.001 Hz) and weakly nonlinear with a height in the range 1 to 2 cm.

Generally, an unwanted free wave having twice the frequency of the first harmonic was observed beating with the bound second harmonic of the regular wave. The experimental setup for generation of a pure regular wave, that is, without any free wave and seiching problem, is described in Appendix A.

The reflective beach consisted of a sloping plane of length $L = 25.5$ cm, transversally placed with one edge on the solid bottom and the other above water. The required partially standing wave field was produced by adjusting the slope of this board. For a given slope, and for waves of frequency 1.5 Hz, the reflection coefficient R_b, that is, the ratio of the reflected wave amplitude to the incident wave amplitude, was found to decrease from 0.45 to 0.1 when the wave height increased. This is due to the enhanced dissipation through the increase of the breaking with the wave amplitude.

The absorbing beach consisted of a similar setup, but with a smaller slope (< 0.05) and a longer length (1 m), in order to dissipate the main part of the incident wave energy through breaking. The reflection coefficient was less than 0.05 regardless of wave frequency and amplitude.

2.2. Wave and Bottom Measurements

The water surface displacement was measured by using an ultrasonic probe (Model E-201, manufactured by Masa Products Corporation). The detection of the bed profile was performed by using an ultrasonic sensor (Model WS25-5, manufactured by Ultran Laboratories, Inc.). After calibration of the systems an accuracy of 0.01 cm for both the wave amplitudes and the bottom location was found. Both detectors were mounted on a carriage which could be translated along the tank by a stepping motor ensuring a great reproducibility of the measuring position. The detectors and the stepping motor were monitored by a microcomputer. The smallest available horizontal displacement corresponding to one step was 0.00456 cm.

For a fixed position, that is, fixed abscissa x along the tank, the surface elevation $\eta(x,t)$ was measured at regular intervals during a total time greater than the wave period $T = 2\pi/\omega$. These records were then subsequently processed through Fourier analysis, by fitting $\eta(x,t)$ to the relation

$$\eta(x,t) = \sum_n A_n(x)\cos(n\omega t + \varphi_n(x)),$$

where $A_n(x)$ is the amplitude and $\varphi_n(x)$ the phase of the envelope of the harmonics of the wave. Note that both the bound second harmonic of the regular wave and the free wave have the frequency 2ω ($n = 2$) and hence cannot be distinguished with this analysis.

The process was repeated for typically 200 positions along the tank for an overall displacement of about 200 cm. The reflection of the first harmonic of the wave by a given profile was obtained by examining the rate of standing wave of the envelope of the first harmonic located upstream of the profile. The locations of the maxima and minima of the wave envelope gave information on the phase of the reflected wave. The rereflected

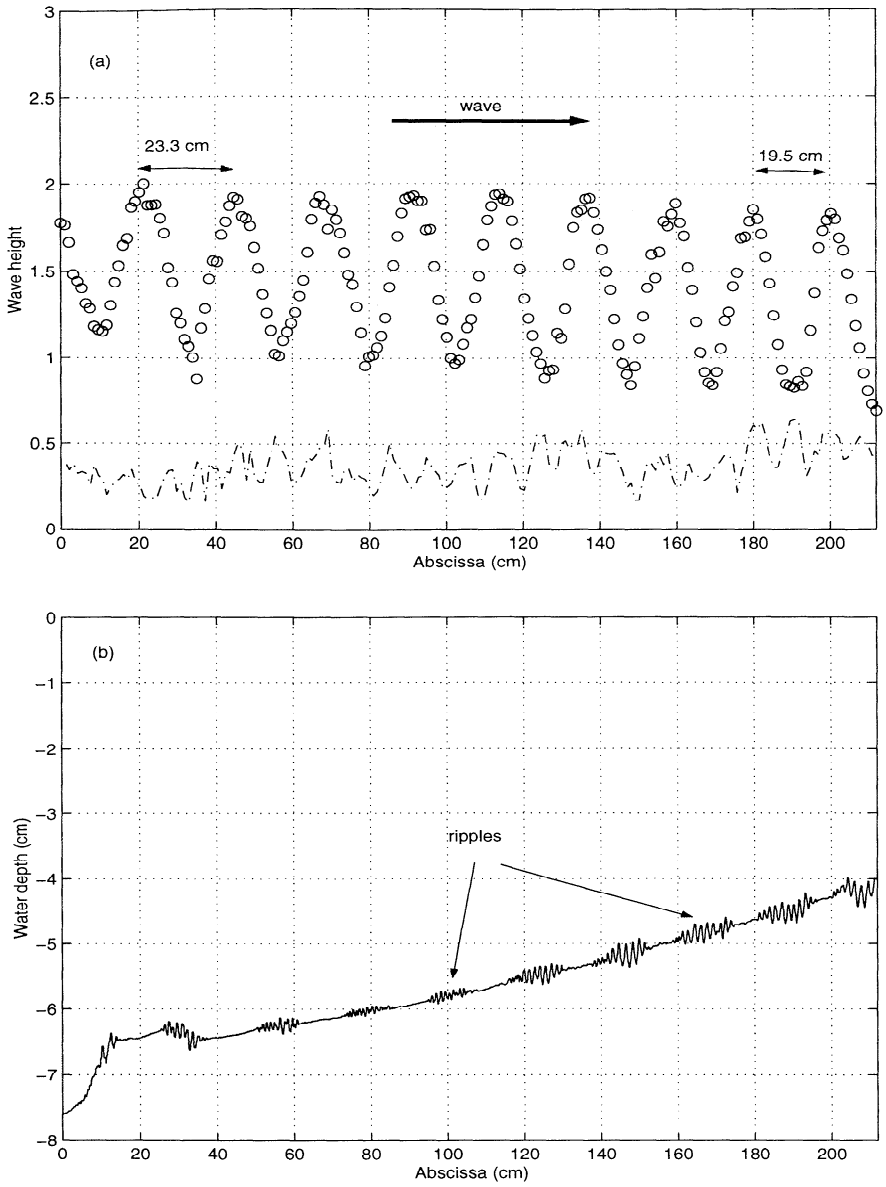

Figure 2. (a) First harmonic (circles) and second harmonic (dashed line) wave components over bathymetric profile and (b) after 300 s of wave action. $H = 1.6$ cm and $R_b = 0.31$.

Table 1. Experimental Interbar Spacing and Wave Envelope Crest to Crest Measurements and Theoretical Wavelength for the Case $H = 1.6$ cm and $R_b = 0.31$

Depth, cm	Interbar Spacing, cm	Wave Envelope Crest to Crest Spacing, cm	Theoretical Wavelength, cm
4.6	19.8	20.1	41.5
4.8	21.2	21.2	42.6
5.2	21.8	21.8	43.8
5.5	22.3	22.4	44.9
5.8	22.9	23.2	45.8
6	23.4	23.4	46.5
6.3	23.9	23.9	47.4
6.3	23.2	23.4	47.4

wave from the wave board may affect the measured reflection coefficient of the bed. This effect was estimated through a numerical simulation using linear potential theory.

The bed profile was measured in between the same abscissa, with a step of about 0.05 cm. The different length scales of the bed profile, small-scale ripples and bars, were analyzed in a power spectrum through fast Fourier transform (FFT). Due to poor FFT resolution, some low-frequency peaks were truncated, but nevertheless their centers were easily identified. In fact, the length of the spatial series of the bottom recording is 212 cm, so the theoretical resolution in the spectrum is of order $1/(2\text{x}212)$ cm $= 0.0024$ cm^{-1}.

3. Results

In the experiments presented hereinafter, bed erosions were carried out for a first harmonic wave frequency $f_0 = 1.5$ Hz. In waters of constant depth, $h = 5$ cm, and for a beach reflection coefficient $R_b = 0.16$, the incipient sediment motion was observed for a wave height of 1.2 cm; in the potential linear theory this corresponds to a near-bed velocity amplitude of $U_0 = 8 \pm 1$ cm s^{-1}. Whatever the beach reflection coefficient R_b, the sloping bed erosions were conducted using weakly nonlinear incident waves, with heights slightly above the erosion threshold. Systematic repetitions of experiments with given initial conditions showed the good reproducibility of the results.

Under the surface wave action, sandbars were formed, with characteristic lengths depending on the surface wave conditions. Their wave reflecting power versus frequency was then studied thanks to experiments carried out with small-wave amplitudes (under the erosion threshold to avoid the bed shape changes) in order to verify Bragg resonances. The results were compared to those of a numerical model based on the linearized potential theory of gravity waves (see *Rey* [1992] for details).

3.1. Case of an Almost Pure Regular Wave

In this first series of experiments we examined the bed erosion under the action of an almost pure regular wave obtained thanks to the sand sill (Appendix A). The incident wave height was $H = 1.6$ cm and the initial reflection coefficient $R_b = 0.31$.

The bed profile obtained after 3×10^2 s of erosion shows the early formation of small-scale vortex ripples which will play the role of sources for the suspended load sediment (Figure 2). These ripples are first located under the nodes, where the near-bed fluid oscillations are the largest. Almost no beating is observed in the envelope of the second harmonic which, moreover, is modulated with a spacing close to the quarter of the local wavelength. This indicates the absence of a free wave and thus we deal with a partially standing regular wave. Moreover, the envelope of the first harmonic of the wave is modulated with a spacing close to half the local wavelength, which is regularly decreasing from 46.5 cm in water depth of 6 cm, to 39.2 cm in water depth of 4 cm (see Table 1). The consideration of the amplitudes of the wave components reveals that this wave is of moderate height (with more than 95% of the wave energy in the first harmonic).

The bathymetry obtained after 7.2×10^4 s of erosion is displayed on Figure 3 with the corresponding wave envelope; the initial profile is also presented. A system of nine well-developed bars can be seen. These formed under the antinodes of the envelope, with an approximately constant amplitude of about 1.2 cm (Figure 3). The interbar spacing was found close to half the local wavelength (Table 1), which corresponds to the first-order Bragg condition. Let us note that a consequence of this Bragg condition is an increase of the wave reflection, evidenced in Figure 3a by an increase of the rate of standing wave upstream of the sandy bed. This behavior is discussed in detail in section 4.3.

The power spectrum of the modulated profile, obtained by subtracting the initial profile from this ultimate profile, is presented in Figure 4 and compared with those of a pseudosinusoidal profile of the form $\delta(x) = a_B \sin 2kx$, where a_B is the bar amplitude, $k(x)$ is the local wavenumber of the surface wave at mean water depth $h(x)$, and x is the abscissa downstream of the start of the sandbed. The good agreement demonstrates clearly a bed modulation satisfying the local Bragg condition. Indeed, in both plots, a sharp peak is found close to the sand bed wavenumber of 0.287 cm^{-1}, corresponding to a length scale of about 22 cm.

In order to verify the Bragg resonance, experiments were conducted with small-wave amplitudes of 0.3 cm; that is, far beneath the erosion threshold, in the frequency range 1 to 2 Hz, and for an almost progressive wave, by using the absorbing beach. The experimental results for the wave reflection due to the modulated bed only (no beach reflection) are displayed in Figure 5 and compared with the linearized numerical simulation using 200 steps for the bottom discretization. The main finding is that experiments and simulations agree in showing a maximum for the reflection coefficient in the vicinity of 1.5 Hz. Then the length scale of 22 cm which is close to half the wavelength at the frequency 1.5 Hz in the mean water depth of 5 cm (43.15 cm) is clearly correlated to a first-order Bragg resonance.

3.2. Influence of the Free Wave

In a second series of experiments, the wave resulted from the superposition of a free wave on a regular wave. The free wave was easily recovered through removal of the sand sill. Consequently, this reduced the total length of the sand bed from 200 to 180 cm. In the typical experiment presented below, the incident wave height was 1.9 cm, and the initial reflection coefficient is 0.42.

Again, a system of nine bars is observed in the ultimate bed profile after 1.2×10^4 s of wave action (Figure 6). As in the previous case, the bar amplitude is about 1 cm, but here the bar spacing is irregularly decreasing with decreasing water depth (Table 2). We will show that this lack of regularity in the bar spacing can be attributed to the free wave.

The presence of the free wave was detected from the envelope of the second harmonic of the wave, through a beating with a local wavelength of 65 ± 5 cm in the region of mean water depth $h \simeq 5$ cm (Figure 6). Indeed, in the linear theory, for the frequency of the first harmonic $f_0 = 1.5$ Hz and water depth $h = 5$ cm, the wavenumber of the first harmonic is $k = 0.1456$ cm^{-1} and the wavenumber of the free wave $K = 0.3789$ cm^{-1}. Hence the beating has a local wavelength given by

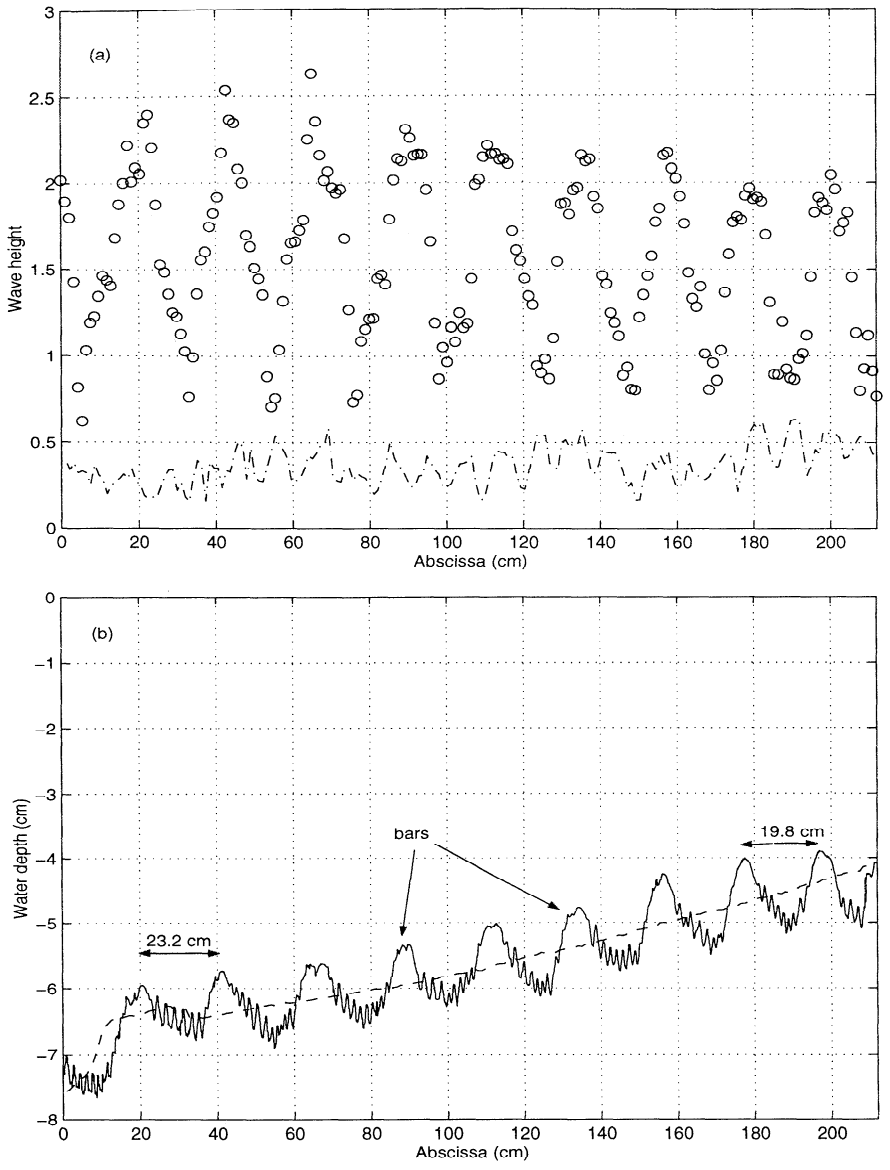

Figure 3. (a) First harmonic (circles) and second harmonic (dashed line) wave components over final bed profile, and (b) initial (dashed) and final (solid) bed profiles. $H = 1.6$ cm and $R_b = 0.31$.

$$\lambda_{\text{beating}} = \frac{2\pi}{K - 2k} = 71.64 \text{ cm} \qquad (1)$$

which is close to the measured value. In addition to this beating, a perturbation of the regular wave by the free wave is observed on the envelope of the first harmonic of the wave, which is not any more modulated by half the local wavelength of the surface wave (Table 2).

The role of the free wave was also analyzed through the power spectrum of the difference between the final and initial profiles. Figure 7 shows that the experimental spectrum reveals two characteristic wavenumbers of the sand bed at 0.283 cm^{-1} (main peak) and 0.390 cm^{-1} (secondary peak).

A first length scale of about 22.2 cm is obtained, which is again associated with the first-order Bragg reflection for the regular wave. The second length scale of 16.1 cm is then associated with the free wave. Indeed, in waters of depth 5 cm, this length scale is related to a Bragg resonance of first-order at a frequency close to 1.86 Hz for which the wavelength is 32.39 cm, or of second order at a frequency close to 3 Hz, that is, the frequency of the free wave for which the wavelength is 16.58 cm. In waters of depth 4 cm the frequency of the first-order Bragg resonance is close to 1.8 Hz.

As a result of first-order Bragg resonance, the reflection coefficient is expected to exhibit not only a main peak at 1.5 Hz but also a peak at 1.83 Hz. This is experimentally confirmed and is also in agreement with the results of the potential model (Figure 8).

3.3. Influence of the Wave Amplitude and of the Initial Rate of Standing Wave

The beach reflection coefficient is expected to depend on the amplitude of the incident nonlinear wave. In fact,

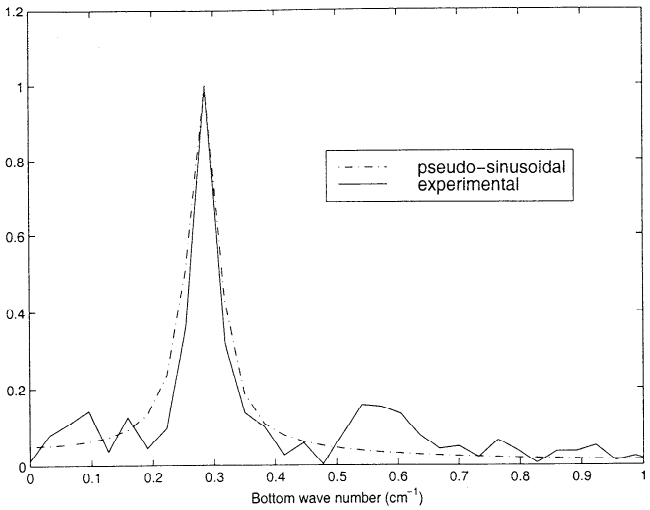

Figure 4. Normalized spectrum of the final experimental and pseudo-sinusoidal bathymetric profiles.

the reflection coefficient decreases with increasing wave amplitude. Hence we did not attempt to carry out the study with an initial reflection coefficient a priori given, but rather we chose to leave the beach slope unchanged and to vary the wave amplitude. In the four experiments presented hereinafter, three were conducted with a beach slope fixed at 0.24 and one with the attenuation beach (slope <0.05), the wave height was varied from 1.2 to 1.7 cm, and the initial reflection coefficient was then found to vary from 0.16 to 0.05. With these small values of amplitudes and reflection coefficients, it was necessary to run the erosion over more than 1.2×10^5 s to obtain the equilibrium profile of the bed.

In the first case, where the wave height was $H = 1.2$ cm and the reflection coefficient was initially $R_b = 0.16$, ripples and bars only formed in the region of water depth smaller than 5 cm (Figure 9). The near-bed orbital velocity was deduced from H and f_0 by using the linear potential theory, and its amplitude was found to be below the erosion threshold everywhere in the noneroded region (Table 3). This is in agreement with the experimental observation that the wave field is not enough energetic to erode the bed in water depth greater than 5 cm (Table 3). In the eroded area the wavelength of the bottom undulations increased with the increasing depth, in accordance with the undulations of the wave envelope (Table 4).

In fact, a beating is observed in the envelope of the second harmonic of the wave, but the presence of the free wave is neither detected in the first harmonic of the wave (Figure 9) nor in the bottom spectrum obtained through FFT analysis (Figure 10). The latter observation may be explained through a broadening of the peaks due to the small extent of the eroded region, where only four bars were formed.

In the second case, the erosion was conducted with $H = 1.35$ cm and $R_b = 0.14$, and nine bars were formed over the whole array of sediment (Figure 11). Here the large beating observed in the envelope of the second harmonic reveals a stronger rate of free wave than in the preceding experiment. Consequently, the long length-scale anomaly in the bar distribution which is observed, as in the experiment of section 3.2, is correlated with the free wave (Table 5).

Indeed, the bottom spectrum displayed in Figure 10 not only shows the two peaks already observed in the similar experiment of section 3.2 but also a third peak at a much lower spatial frequency. This peak, of which the maximum is not obtained due to poor FFT resolution, is centered around a spatial frequency of the order of 0.0123 cm^{-1}, which means a length of

$$L_{\mathrm{FFT}} = (0.0123 \text{ cm}^{-1})^{-1} = 77 \text{ cm} \qquad (2)$$

with an estimated error of $\pm$ 5 cm. The lengths of beating, $\lambda_{\mathrm{beating}}$, are 85 ± 5 cm for a water depth between 4 and 5 cm, and 60 ± 5 cm for a deeper water, which is close to the mean value of $\lambda_{\mathrm{beating}}$. The beating between the free wave and the bound second harmonic of the regular wave is thus revealed by this low spatial frequency peak.

The experiment presented in the third case was conducted with $H = 1.65$ cm and $R_b = 0.1$. Again a strong rate of free wave was expected from the beating in the second harmonic of the wave, but the bars formed with a spacing of a much larger size than half the local wavelength, obviously of the same order as the length of beating (Figure 12). The standard modulation with two peaks in the bottom spectrum has then been replaced by a modulation of larger length scale. In fact, the bottom spectrum (Figure 10) clearly shows that the vanishing of the two peaks is associated with a considerable increase in the low-frequency peak corresponding to the length of beating.

Observations of these three cases show the transition from a case, where the bottom spectrum is dominated

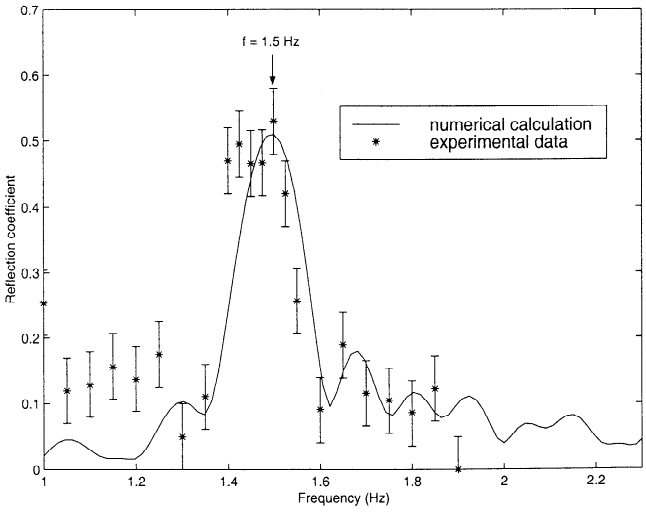

Figure 5. Reflection study with the purely monochromatic wave.

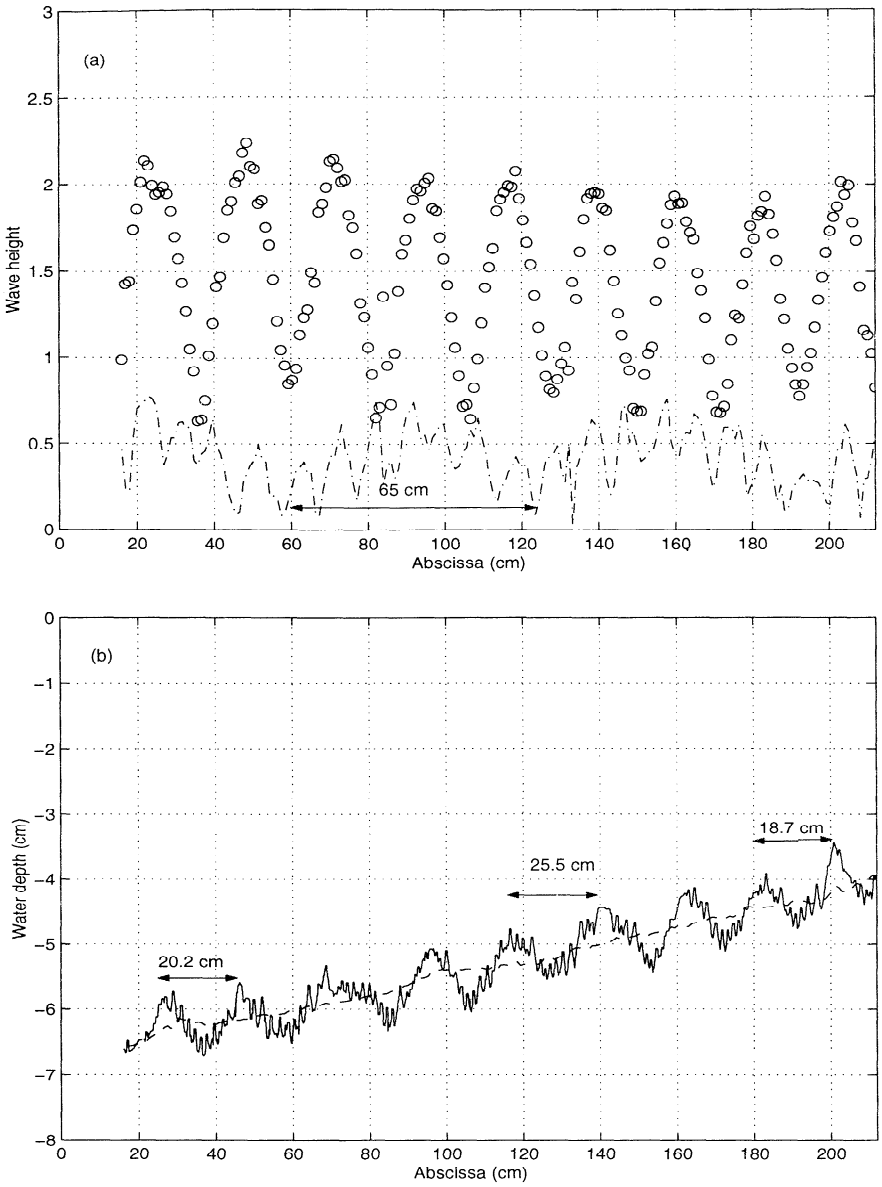

Figure 6. As for Figure 3, but for $H = 1.9$ cm and $R_b = 0.42$.

by the wavenumber of the first harmonic (small amplitude) to a case where the bottom profile mainly reproduces the beating of the envelope of the second harmonic (large amplitude and small reflection coefficient).

This was confirmed in a fourth experiment where the reflective beach was replaced by the attenuation beach for which the reflection coefficient was 0.05 for a wave height $H = 1.7$ cm. The final profile and the final envelope of the second harmonic are presented in Figure 13. A similar situation as in case 3 is recovered, but with a translation of the whole bar patch. As the location of the attenuation beach was downstream of that of the reflection beach, a phase lag resulted in the wave envelope between both experiments, which was clearly observed to be reproduced in the bottom undulations.

Table 2. Experimental Interbar Spacing and Wave Envelope Crest to Crest Measurements and Theoretical Wavelength for the Case $H = 1.9$ cm and $R_b = 0.42$

Depth, cm	Interbar Spacing, cm	Wave Envelope Crest to Crest Spacing, cm	Theoretical Wavelength, cm
4.4	18.7	19.5	40.8
4.6	19.1	20.5	41.6
4.8	22.4	21.5	42.4
5.1	24.5	23.3	43.5
5.3	21.9	21.5	44.2
5.7	23.8	23.4	45.5
6	24.5	24.3	46.5
6.1	19.2	20.5	46.8

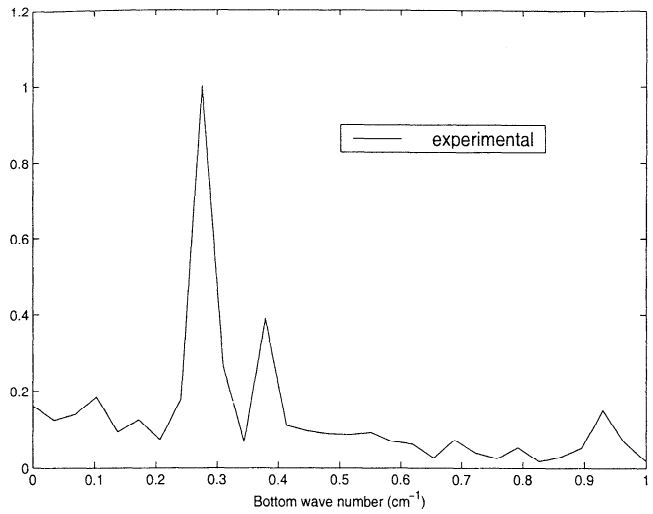

Figure 7. Normalized spectrum of the final experimental bathymetric profile (presence of the free wave).

4. Discussion

4.1. Wave Field Characteristics

In earlier studies [*Rey et al.*, 1995], our experimental setup showed good capabilities for modeling the sediment transport under wave action. In the present series of experiments we had to control the characteristics of the generated wave field, in terms of initial rate of standing wave, free wave amplitude, and rereflection from the wave flap.

1. The initial rate of standing wave was obtained through the choice of the beach (plane board of adjustable slope or absorbing beach) but was also found to depend on the wave height.

2. The presence of an unwanted free wave is a serious problem in laboratory wave generation because such a spurious wave is generally difficult to separate from the expected wave which it perturbs. The free wave is not only produced by a sinusoidally moving wave flap but may also be generated when a wave is incident over a bottom region of locally large steepness. The control of the free wave is exposed in Appendix A.

3. The rereflection from the wave board had two main consequences. The first one is a systematic error in the measured reflection coefficient. The wave maker was modeled using a linear potential model, and the role of the rereflection was numerically estimated. As a result, for a bed reflection coefficient as large as 0.6, the induced relative error is found less than 0.15. The second consequence is that seiching may be induced. It was strictly necessary to suppress an initial seiching which would prevent any bar formation. This was obtained either through a careful positioning of the reflective beach with respect to the wave board, or by using a filter (Appendix A).

4.2. Wave Envelope and Bed Spatial Modulations

According to the model of bar formation outside the breaking zone, presented in the introduction [*O'Hare and Davies*, 1993], the spatial modulation of the envelope of the first harmonic of the wave dominates the sediment redistribution and is reproduced in the eroded bed. This was observed in recent experiments for partially standing waves over sandy beds of initially constant depth [*O'Hare and Davies*, 1990; *Rey et al.*, 1995], where bars formed with a spacing of half the wavelength of the surface wave, corresponding to the spatial modulation of the envelope of the first harmonic of the wave due to the initial condition of the partially reflecting beach. In the present study the role of the resulting envelope of the first harmonic on the bar formation was addressed also in the case where the bed is initially a sloping plane. This was done with different initial wave field compositions corresponding to different choices of the incident wave (regular wave eventually added with another free wave) and of the beach reflection coefficient (modulus and phase lag). Hence we first modeled the incident wave field, and then we modeled the resulting wave field for a given reflective beach.

The regular wave perturbed by a free wave can be modeled by using *Madsen and Sørensen*'s [1993] results, which are detailed in Appendix B, where the incident wave on the sloping bed is given by

$$\begin{aligned}\eta_1(x,t) &= a\cos(\omega t - \int k dx) \\ &\quad + A_f \cos(\omega t - \int (K-k)dx + \varphi_f) \\ &\quad + a_2 \cos 2(\omega t - \int k dx) \\ &\quad + a_f \cos(2\omega t - \int K dx + \varphi_f), \end{aligned} \tag{3}$$

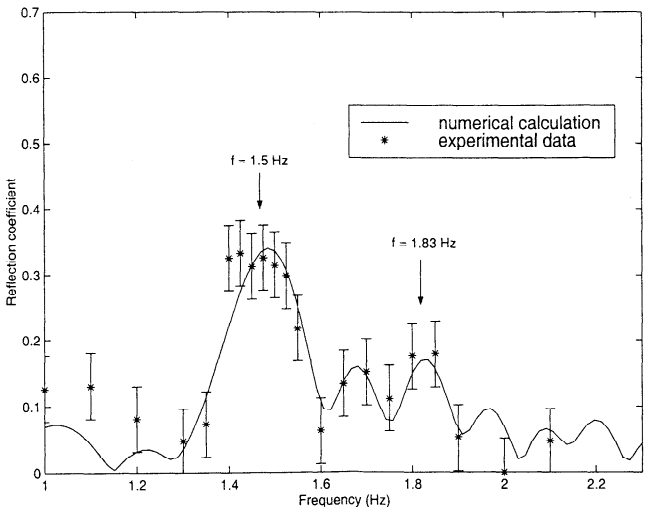

Figure 8. Reflection study with the bimodal wave.

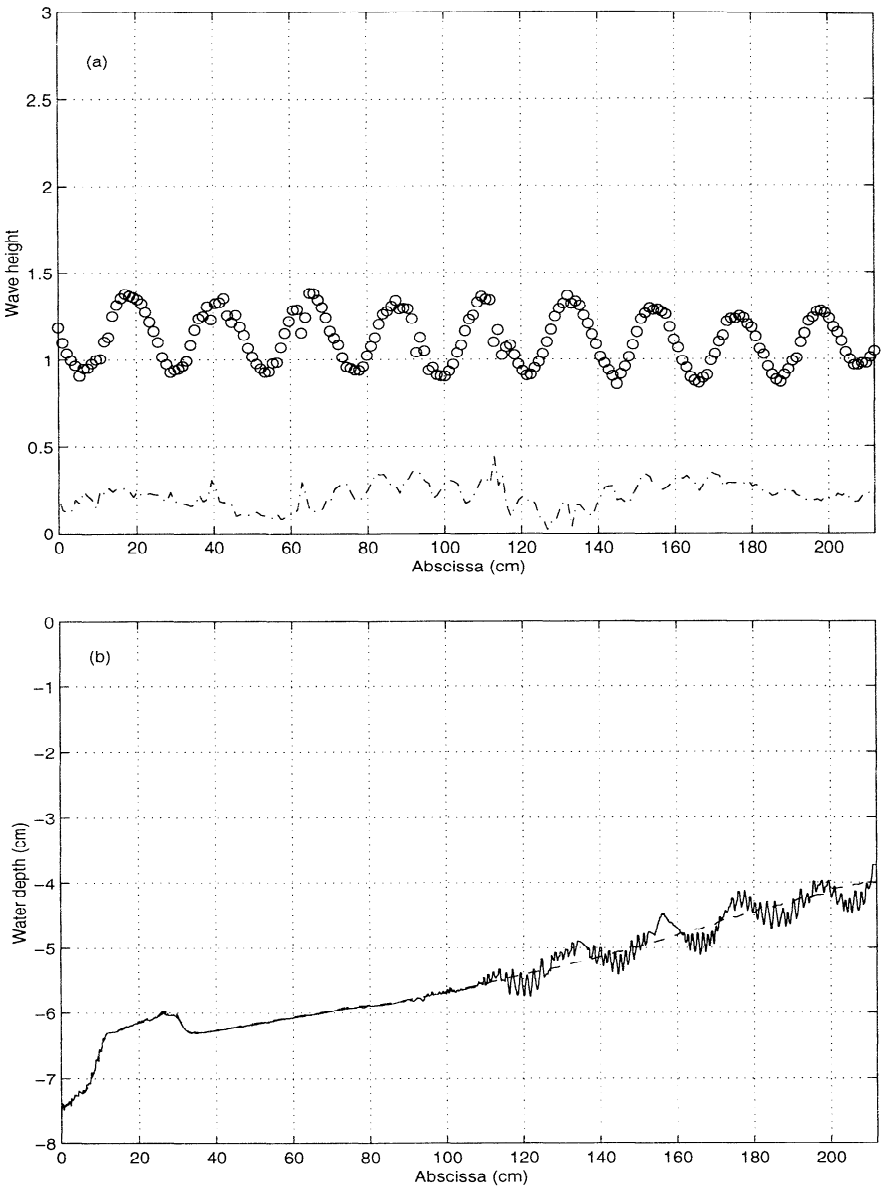

Figure 9. As for Figure 3, but for $H = 1.2$ cm and $R_b = 0.16$.

where $a\cos(\omega t - \int k dx)$ and $a_2 \cos 2(\omega t - \int k dx)$ are the first harmonic and the second harmonic of the regular wave, respectively, $\int k dx$ is the phase lag at abscissa x, and $a_f \cos(2\omega t - \int K dx + \varphi_f)$ is the free wave. The nonlinear difference interaction between the components of the bichromatic resulting wave is expressed in the term $A_f \cos(\omega t - \int (K - k) dx + \varphi_f)$.

Table 3. Maximum Near-Bottom Orbital Velocity Under Nodes (U_N) and Antinodes (U_A) Calculated for Different Wave Field Conditions

	$h = 6$ cm	$h = 5$ cm	$h = 4$ cm
$H = 1.2$ cm	$U_n = 7.3$	$U_n = 8.3$	$U_n = 9.6$
$R = 0.16$	$U_A = 5.3$	$U_A = 5.9$	$U_A = 6.9$
$H = 1.35$ cm	$U_n = 8$	$U_n = 9.1$	$U_n = 10.6$
$R = 0.14$	$U_A = 6$	$U_A = 6.9$	$U_A = 8$
$H = 1.65$ cm	$U_n = 9.5$	$U_n = 10.8$	$U_n = 12.5$
$R = 0.1$	$U_A = 7.7$	$U_A = 8.8$	$U_A = 10.2$
$H = 1.7$ cm	$U_n = 9.3$	$U_n = 10.6$	$U_n = 12.3$
$R = 0.05$	$U_A = 8.4$	$U_A = 9.6$	$U_A = 11.1$

velocity in cm s^{-1}.

As the bed steepness is small, the incident wave is only reflected by the beach. The resulting partially standing wave field of first harmonic amplitude is thus

$$\begin{aligned} \eta^{(\omega)}(x,t) \;=\; & a\left[\cos(\omega t - \int k dx) + R_b \cos(\omega t + \int k dx + \varphi)\right] \\ & + A_f\left[\cos(\omega t - \int (K-k) dx + \varphi_f) + R_b \cos(\omega t + \int (K-k) dx + \varphi_f + \varphi)\right] \end{aligned} \tag{4}$$

where R_b is the modulus of the beach reflection coeffi-

Table 4. Experimental Interbar Spacing and Wave Envelope Crest to Crest Measurements and Theoretical Wavelength for the Case $H = 1.2$ cm and $R_b = 0.16$

Depth, cm	Interbar Spacing, cm	Wave Envelope Crest to Crest Spacing, cm	Theoretical Wavelength, cm
4.3	19.5	20	40.6
4.7	20.9	20.5	42
5	22.3	21.9	43.1
5.3	-	22.8	44.2
5.6	-	23.3	45.2
5.9	-	23.7	46.2
6.1	-	23.3	46.8
6	-	22.8	46.5

cient and φ is the phase lag between incident and reflected waves. By expanding the cosines and collecting the $\cos\omega t$ and $\sin\omega t$ terms, this first harmonic amplitude can also be written as

$$\eta^{(\omega)}(x,t) = C(x)\cos\omega t + S(x)\sin\omega t, \tag{5}$$

where

$$\begin{aligned} C(x) &= a\left(\cos(\int k dx) + R_b\cos(\int k dx + \varphi)\right) \\ &+A_f\left(\cos(\int (K-k)dx - \varphi_f)\right. \\ &\left.+R_b\cos(\int (K-k)dx - \varphi_f - \varphi)\right) \end{aligned} \tag{6}$$

$$\begin{aligned} S(x) &= a\left(\sin(\int k dx) - R_b\sin(\int k dx + \varphi)\right) \\ &+A_f\left(\sin(\int (K-k)dx - \varphi_f)\right. \\ &\left.-R_b\sin(\int (K-k)dx - \varphi_f - \varphi)\right). \end{aligned} \tag{7}$$

Then the envelope of the first harmonic becomes

$$A^{(\omega)}(x) = \left(C(x)^2 + S(x)^2\right)^{1/2}. \tag{8}$$

After some calculations, (8) becomes

$$\begin{aligned} A^{(\omega)}(x) &= \left[a^2\left(1 + R_b^2 + 2R_b\cos(2\int k dx + \varphi)\right)\right. \\ &+A_f^2\left(1 + R_b^2\right. \\ &\left.+2R_b\cos(2\int (K-k)dx + \varphi)\right) \\ &+2aA_f\left(\cos(\int (K-2k)dx - \varphi_f)\right. \\ &+2R_b\cos\varphi_f\cos(\int K dx + \varphi) \\ &\left.\left.+R_b^2\cos(\int (K-2k)dx + \varphi_f)\right)\right]^{\frac{1}{2}}. \end{aligned} \tag{9}$$

However, since $O(A_f^2) = (a_f^2 a^2)/h^2 \ll O(aA_f) = (a_f a^2)/h$, the envelope of the first harmonic of the wave becomes of leading order

$$\begin{aligned} A^{(\omega)}(x) &= a\left[1 + R_b^2 + 2R_b\cos(2\int k dx + \varphi)\right. \\ &+\frac{2A_f}{a}\left(2R_b\cos\varphi_f\cos(\int K dx + \varphi)\right. \\ &+\cos(\int (K-2k)dx - \varphi_f) \\ &\left.\left.+R_b^2\cos(\int (K-2k)dx + \varphi_f)\right)\right]^{\frac{1}{2}} \\ &+O\left(\frac{aa_f^2}{h^2}\right), \end{aligned} \tag{10}$$

where $O(A_f/a) = a_f/h$.

Three modulations are found in this envelope: a first-order modulation of local wavenumber $2k$ and two second-order modulations, one of local wavenumber K and the other of local wavenumber $K-2k$. The relative weight of the different modulations is found to depend upon both the beach reflection coefficient R_b and the free wave characteristics. Hence for a partially standing pure regular wave ($R_b \neq 0$ and $a_f \to 0$, section 3.1) the only modulation is the first-order one, of local wavenumber $2k$.

On the contrary, for a progressive bimodal wave ($R_b \to 0$ and $a_f \neq 0$), the only modulation is the secondary modulation of local wavenumber $K - 2k$ (section 3.3). Observation of the bed profile's spectrum shows that this modulation is more and more pronounced in regard to the other ones as R_b decreases from 0.16 to 0.1 (Figure 10). The characteristic length of this modulation, that is, the beating length, is the unique length scale of an envelope of a progressive wave. Indeed, in the limiting experimental case with $R_b = 0.05$, that is,

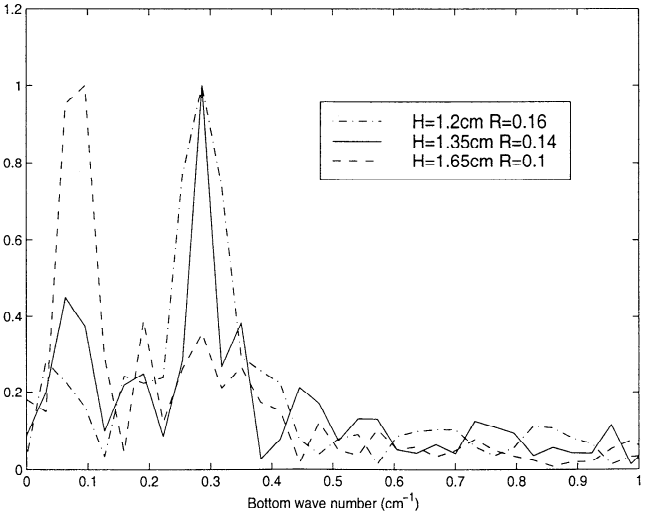

Figure 10. Normalized spectrum of the three different final profiles obtained with low beach reflection.

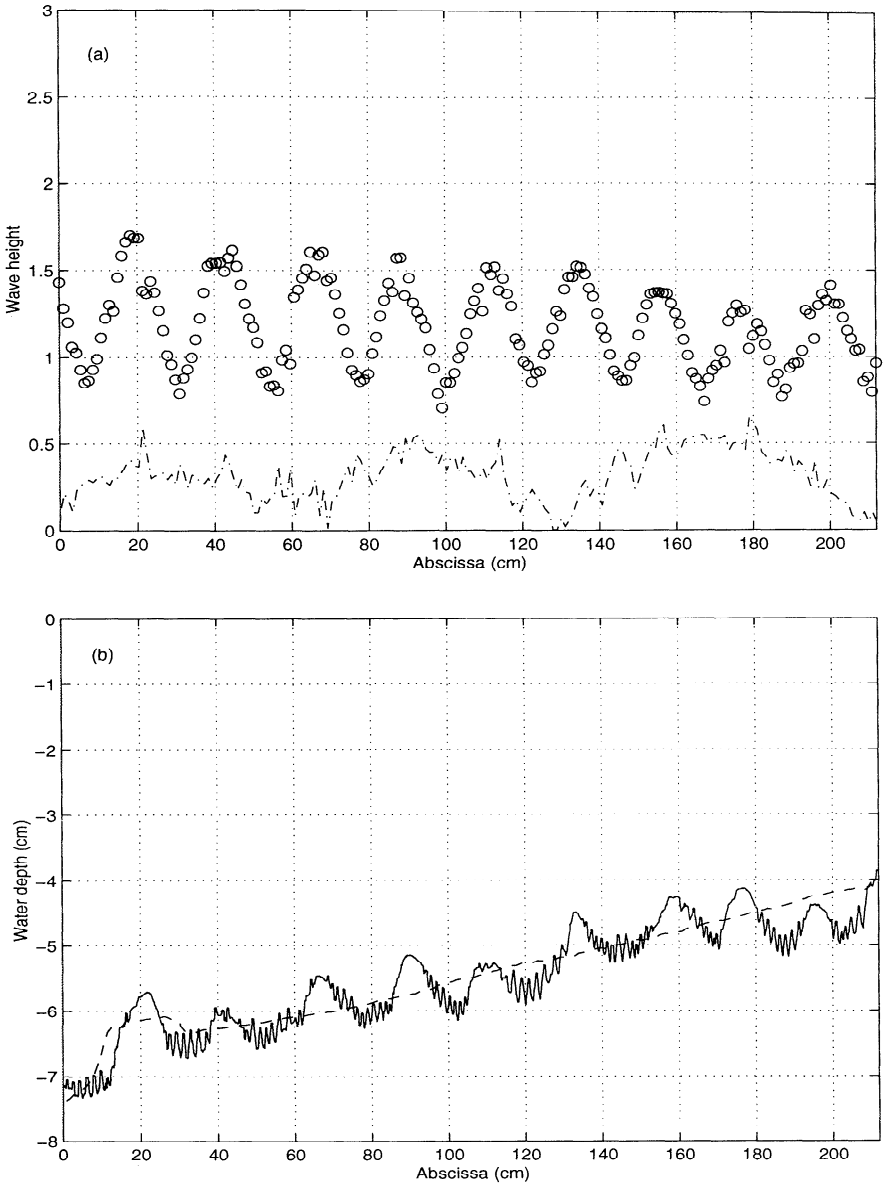

Figure 11. As for Figure 3, but for $H = 1.35$ cm and $R_b = 0.14$.

Table 5. Experimental Interbar Spacing and Wave Envelope Crest to Crest Measurements and Theoretical Wavelength for the Case $H = 1.35$ cm and $R_b = 0.14$

Depth, cm	Interbar Spacing, cm	Wave Envelope Crest to Crest Spacing, cm	Theoretical Wavelength, cm
4.4	18.8	19	40.8
4.6	17.4	17.3	41.6
4.9	23.5	23.1	42.8
5.3	24.4	24.4	44.2
5.6	19.7	20.6	45.2
5.9	23	23.1	46.2
6.1	24.4	24.9	46.8
6.2	19.7	20	47.1

for an almost progressive wave, this beating length is recovered as unique in the final bed profile (Figure 13). For a high initial rate of standing wave, and in the presence of a free wave, both modulations corresponding to the wavenumbers $2k$ and K are observed (section 3.2). The comparison of the results with the first harmonic amplitude given by (10) seems to confirm that the bar formation is controlled by the envelope of the first harmonic of the wave even if perturbed by a free wave. Let us note that in the results presented in section 3.3 we observed that the eroded bed profile reproduced the envelope of the second harmonic, which modulation was also present in the first harmonic. In fact, the higher harmonic wave components may also contribute in the sediment redistribution, but only through the perturbation of the first harmonic. The sediment extraction, its

redistribution, and finally the ultimate bed modulation are dominated by the modulations of the first harmonic component of the wave.

For a wave propagating in finite water depth, these bed modulations may reflect a significant part of the wave energy at the Bragg resonances. These resonance conditions were found by examining the spectrum of the final experimental bathymetric profile. They were revealed by measuring the reflection coefficient of the eroded bed in isolation, that is, with an absorbing beach, and for low-amplitude waves. For such linear waves, the bed was frozen as the wave amplitude was under the erosion threshold. Linear reflection coefficient measurements were found in good agreement with numerical results of the linear potential model. This is due to the quasilinear behavior of the erosion process in the present study. For the experimental measurements, the error was about $\pm$ 0.05, and there was a relatively strong reflection coefficient in the lowest frequency range (1 – 1.2 Hz) due to the imperfections of the absorbing beach. We can conclude in terms of Bragg resonance for the present experiments:

1. In the particular case of a partially standing almost pure regular wave ($R_b = 0.31$ and $a_f \approx 0$), a formation of sand bars is observed with an interbar spacing satisfying the local Bragg condition $K_B = 2k$. In fact, the spectrum of the experimental bed profile is found in good agreement with the one of a sinusoidal profile of local wavenumber $2k$. As expected from this Bragg condition, the experimental low-amplitude wave reflec-

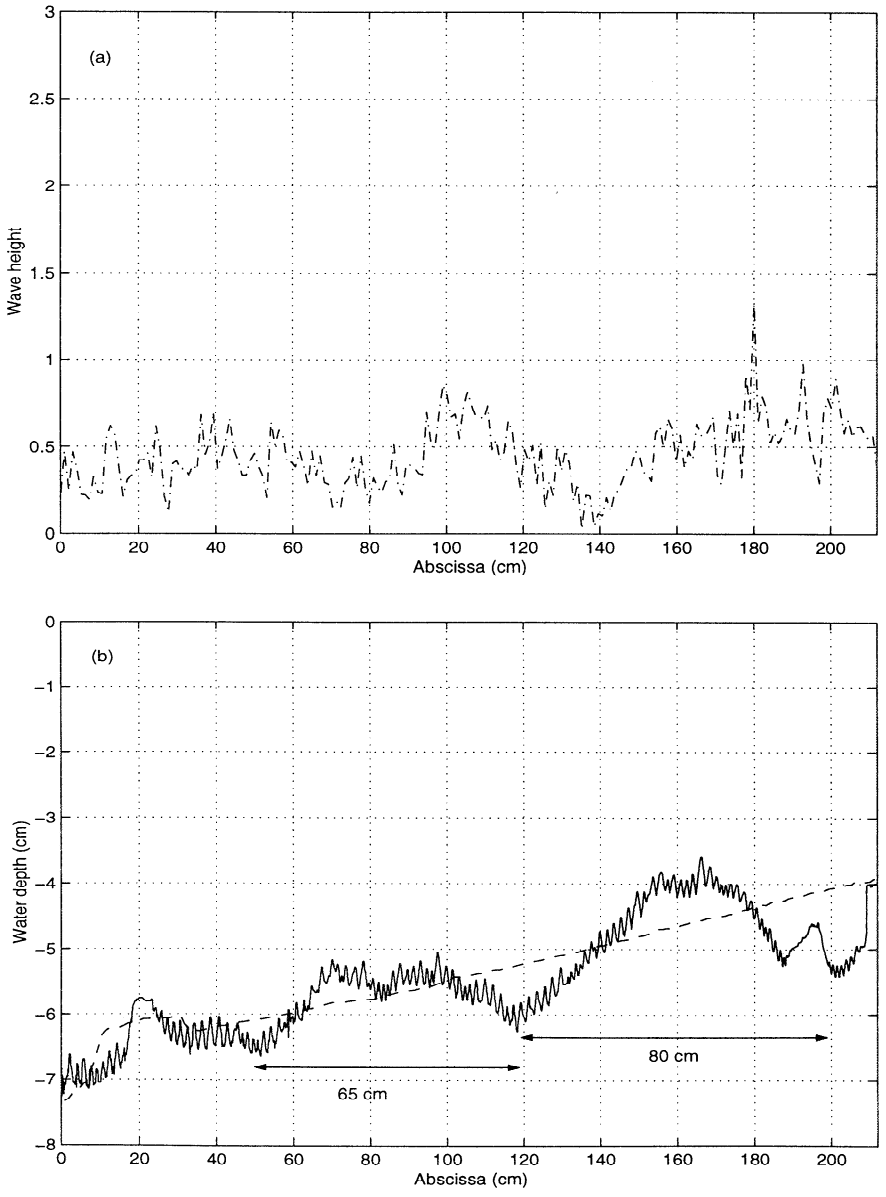

Figure 12. (a) Second harmonic wave component over final bed profile, (b) initial (dashed) and final (solid) bed profiles. $H = 1.65$ cm and $R_b = 0.1$.

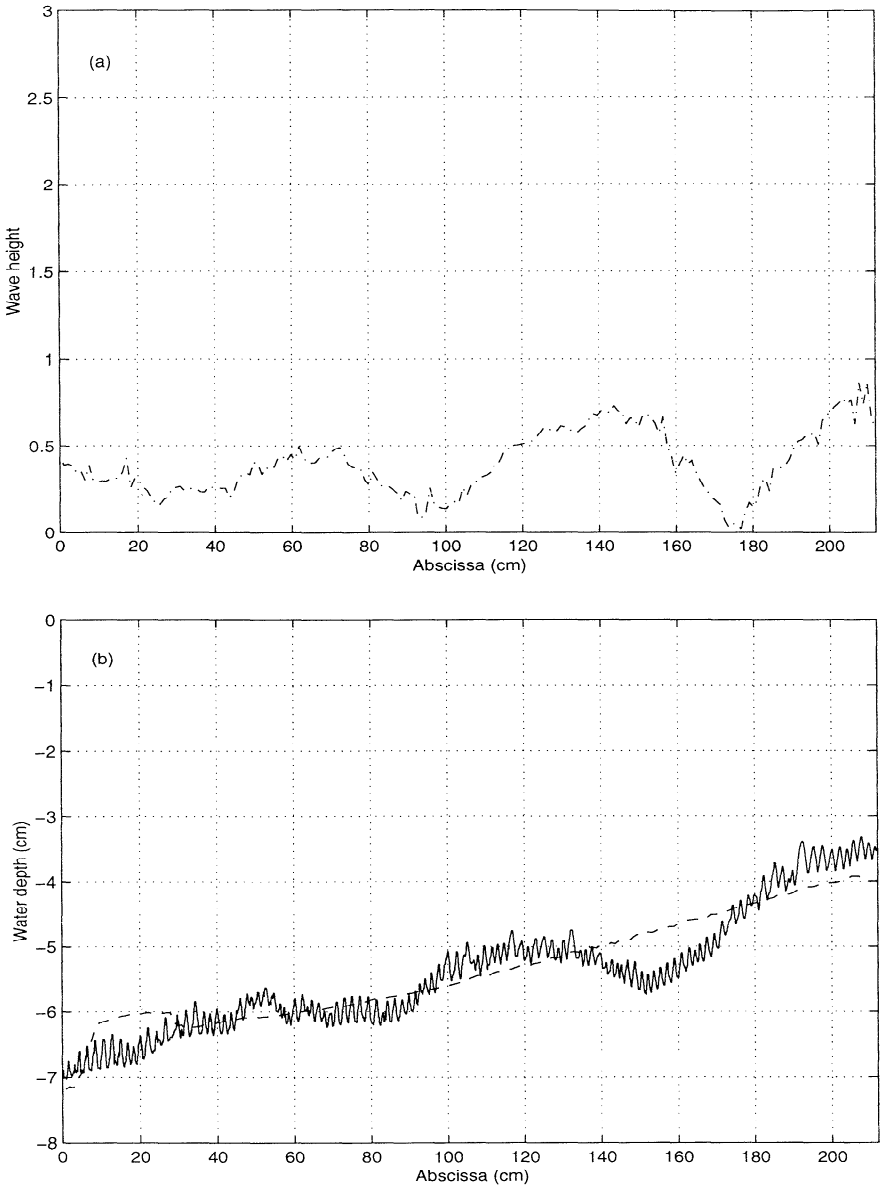

Figure 13. As for Figure 12 but for $H = 1.7$ cm and $R_b < 0.05$.

tion coefficient of the bar system is maximum near the eroding wave frequency $f_0 = 1.5$ Hz. These experimental data are in good agreement with the numerical calculations based on the linear potential model.

2. In the general case of a bimodal wave ($a_f \neq 0$), different modulations are observed according to the beach reflection coefficient R_b. First, for a high initial rate of standing wave ($R_b = 0.42$ for a wave height $H = 1.9$ cm), both local modulations $2k$ and K are observed, two first-order Bragg resonances are then expected at both wavenumbers $k' = k$ or $k' = K/2$. These are effectively revealed from measurements of the (linear) reflection coefficient, due to the bed, of low-amplitude waves, through two peaks at frequencies $f_0 = 1.5$ Hz ($k' = k$) and $f = 1.83$ Hz ($k' = K/2$). This is confirmed by the numerical simulation. We notice that the second-order Bragg resonance $k' = K$ is not observed since the modulation of wavenumber K is of second order and due to the poor wave-bed coupling at frequency 3 Hz. Second, the secondary modulation of local wavenumber $K - 2k$ is revealed as the initial rate of standing wave is weak, as expected from (10). A first-order Bragg resonance is then expected at local wavenumber $k' = (K - 2k)/2$. This is well confirmed by calculating the bed reflection coefficient, which is found to be resonant at the corresponding frequency of 0.5 Hz, that is, quite different from the eroding wave frequency f_0.

4.3. Dynamics of the Bar System Formation

There is a continuous adaptation between the wave and the bottom. After some time of wave action, vortex ripples are observed beneath the nodes of the wave envelope (Figure 2). This shows that in the early de-

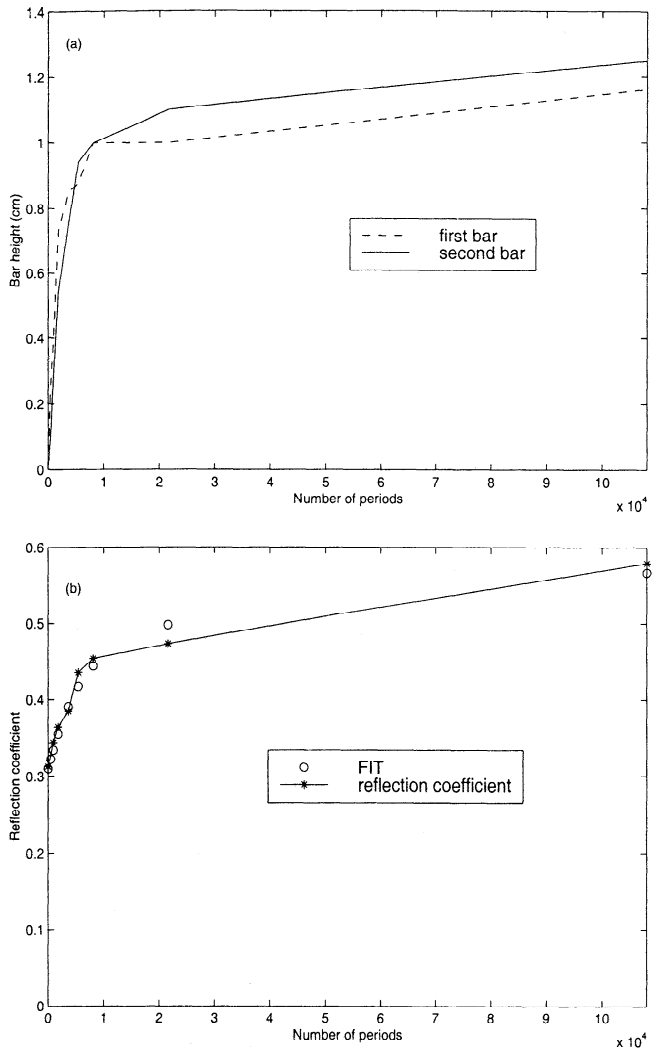

Figure 14. (a) Bar height and (b) reflection coefficient evolution. $H = 1.6$ cm and $R_b = 0.31$.

velopment of the erosion the erodible bed fits the wave. The near bed velocity amplitude U_0 is estimated using the linear potential theory, and then the orbital diameter of the near bed fluid particles $d_0 = U_0/f$ is obtained from the relation:

$$d_0 = \frac{H}{\sinh(kh)}. \tag{11}$$

The mean value of the ripples wavelength l is compared to d_0. In this first series of experiments, with $H = 1.6$ cm, $R_b = 0.31$, and after 300 s of wave action, the value of $l = 1.7$ cm was found by averaging l in the 5 cm water depth eroded region. Hence $l/d_0 = 0.64$ which is closed to the value of 2/3 obtained by *Lofquist* [1978], or of 0.65 obtained by *Miller and Komar* [1980] under oscillatory flow conditions but at much larger scale. The scaling of the ripple wavelength was already obtained by *Rey et al.* [1995], where the scaling of l/ζ, where ζ is the mean ripple height, was also demonstrated.

As the erosion proceeds, the bottom condition forces the wave to fit the bed which itself is evolving under the wave action. For partially standing waves, this coupling is the strongest since the first-order Bragg condition for the eroded bed corresponds to the frequency of the surface wave. The bar formation is governed by the wave height H and the beach reflection coefficient R_b, which is in fact also a function of the wave height. Initially, the beach reflection induces a spatial modulation of the near-bed orbital velocity, with the higher velocities being located under the nodes and the lower ones beneath the antinodes of the wave envelope. With an increasing reflection coefficient, the near-bed velocity is increasing under the nodes and decreasing under the antinodes. If the wave height is close to the threshold value, the erosion areas are regularly spaced (section 3.1). But if the wave height is important and the reflection coefficient is small, the near bed orbital velocity may be greater than the threshold, also under the antinodes. Then the velocity remains spatially modulated, but the erosion areas are no more modulated and the whole bed is eroded (section 3.3).

The wave bed self adjusting, which could be observed at any time of the bed erosion, is experimentally revealed by sampling the time evolution of the reflection coefficient R (Figure 14) for the experiment of section 3.1. This evolution was followed over more than 20 hours, that is, for more than 10^5 wave periods. The behavior of R versus the adimensional time $\tau = t/T$, where T is the wave period, shows that the dynamic is abruptly slowed down after the formation of the first bars, that is, after a time on order of 6000 wave periods. This is confirmed by fitting $R(\tau)$, using two adimensional time constants τ_1 and τ_2, to

$$R(\tau) = R_\infty - \frac{R_\infty - R_0}{2}\left(e^{-\frac{\tau}{\tau_1}} + e^{-\frac{\tau}{\tau_2}}\right), \tag{12}$$

where $R_0 = R(\tau = 0)$ and $R_\infty = R(\tau \to \infty)$.

The best fit was obtained for $R_0 = 0.31$, $R_\infty = 0.65$, $\tau_1 = 6000$, and $\tau_2 = 125,000$. As a result of this, the erosion should have been run over a much longer time, in order to study an hypothetical dynamic equilibrium.

This study clearly shows how more and more bars participate in the wave reflection as the erosion proceeds, the reflection coefficient increasing in the same way as the bars growth. Indeed, the bars initially developed, located in the shallower region, are responsible for the early increase of the reflection coefficient (Figure 14). Finally, the reflection coefficient increased from 0.31 to more than 0.50. This shows that the bars shelter the shore from the impact of the waves at the origin of their formation for a given reflective beach condition. The role of the characteristics of the reflective beach on the reflective power of a bar system has been recently analyzed [*Yu and Mei,* 2000b], showing that shoreline protection with artificial bars based on Bragg reflection is not a simple task.

Since wave bottom interactions are the largest in the shallower waters, bars first formed at the upper part of the slope. If the threshold conditions are only verified for the shallower waters, bars may form only at the upper part of the slope (see Figure 9). The reflecting power of modulated sloping beds is thus mostly due to the modulations at the upper part. The influence of the number of oscillations on sloping beds was analytically studied by using perturbation methods [*Mei*, 1985; *Mei et al.*, 1988], and, for given sinusoid amplitude and slope, the evolution of the reflection coefficient with an increase of the number of offshore bars was found to tend toward a limit.

5. Perspective

In further work, this study will be extended to higher-amplitude waves or to waves with discrete frequency spectrum, where the role on the bar formation of the energy transfer toward low frequencies could be addressed. In a simple case the basic wave field is a wave of frequency f_1 and amplitude a_1 superimposed on a wave of frequency $f_2 > f_1$ and amplitude $a_2 \approx a_1$. As result of nonlinear wave-wave interaction, and retaining only the first-order correction, terms of frequency $2f_1$, $2f_2$, $f_1 + f_2$, and $f_2 - f_1$ are then expected superimposed on the bichromatic weakly nonlinear basic wave field. In the shallow water regime, the action on the bed of the long-wave component of frequency $f_2 - f_1$ could also be observed and compared with the predictions of the wave field model. The case of higher amplitude waves either monochromatic or bichromatic will be also investigated with consideration of shoaling and breaking on emerging sandbeds.

Appendix A: Experimental Setup for a Pure Regular Wave Generation

A.1. Control of the Free Wave

The free wave was generated mainly by the paddle but can be also generated by rapidly varying water depth [*Hulsbergen*, 1974; *Madsen*, 1971]. Several methods [*Hulsbergen*, 1974; *Madsen*, 1971; *Flick and Guza*, 1980] were proposed to damp such free waves.

Madsen [1971] developed an approximate second-order wave maker theory for long-waves of moderate height. He showed that a pure regular wave is generated if the wave maker is given a motion reproducing the fluid particle motion under the required wave of first harmonic frequency f_0. This is obtained when the wave board displacement is given by

$$X(t) = A_0 \sin 2\pi f_0 t + B(A_0) \sin 4\pi f_0 t$$

with the prescribed amplitudes. Unfortunately, our experimental parameters were out of the range of applicability of this method.

The wave maker was immersed in water of depth 6 cm and the generated bimodal wave was then propagated over a step in water depth of 8 cm. As a result, the free wave was significantly reduced downstream of the step, where almost no beating was observed. In this way, an almost pure regular wave was obtained in the region of 8 cm water depth. This region was then connected downstream with the beginning of the sand bed, where the water depth is 6 cm over a 60 cm distance. This was done by either using a plane board or a sill as proposed by *Hulsbergen* [1974]. In the first case the incident wave was transformed into a bimodal wave through production of free wave by the relatively steep slope (0.04) of the plane board. In the second case, no free wave was released. Although the presence of the free wave is revealed through observation of a beating in the envelope of the second harmonic, a more comprehensive analysis is required. *Grue* [1992] proposed a method to extract the free wave amplitude from the envelope of the second harmonic of the wave. However, this method which assumes a constant water depth and does not take into account the nonlinear interactions between the first harmonic and the free wave cannot be applied to our experimental case. *Brossard and Hémon* [1995] proposed to use the Doppler effect to dissociate both waves, owing to their different phase velocities, but this method is chiefly useful for constant depth. To resume, the control or even the detection of the free wave in a wave tank is not very easy and requires a lot of experimental approaches.

A.2. Control of the Seiche

As there was no active wave absorption capability at the wave board, the reflected waves were rereflected from the paddle, eventually leading to long-wave oscillations in the tank. The location of the reflective beach was then carefully adjusted at the beginning of each experiment in order to avoid this seiching. During the erosion, however, the bars grew and participated actively in the wave reflection, therefore a seiche could also be created in the long term. Hence, a 5 cm wide filter made of porous material (loose-compacted fibers) was used between the paddle and the erodible bed. A transmission coefficient T_f of order of 0.6 for the filter was found to avoid seiching, with a very good efficiency for moderate wave heights. In fact, large wave heights ($H > 1.7$ cm) were obtained only by removing the filter. Then the location of the reflective beach was carefully selected with respect to the wave board, in order to avoid an initial seiching which would prevent any bar formation. However, in the case of the largest wave height ($H = 1.9$ cm), a seiching was always observed after the long-term bed erosion, that is, for already well-developed bars. Nevertheless, the occurrence of such a seiching did not prevent the subsequent development of the bar system; at most it slowed down the process. This seiching is obviously a consequence of the bar formation. Indeed, the amplitude of the reflected wave increases as the bars grow, and owing to the selectivity of the reflection coefficient, the wave composition is changed as compared to

the initial situation. This wave distortion negates the matching condition initially obtained at the wave board and triggers the seiching.

Appendix B: Bimodal Wave Modeling

The propagation of a one-dimensional weakly nonlinear surface wave over an uneven bottom has been recently addressed by *Madsen and Sørensen* [1993]. The wave is propagating in the horizontal direction x in a still water depth $h(x)$ and the surface elevation at time t is $\eta(x,t)$. A new form of the Boussinesq equations is derived which leads to the approximate relation

$$L(\eta) = M(\eta) + N_{xx}(\eta), \tag{B1}$$

where L and M, linear operators, and N, nonlinear (quadratic) operator, are given by

$$L = \left(\eta_{tt} - gh\eta_{xx} + Bgh^3\eta_{xxxx} - \left(B + \frac{1}{3}\right)h^2\eta_{xxtt}\right), \tag{B2}$$

$$M = \left(g\eta_x + (2B+1)h\eta_{xtt} - 5Bgh^2\eta_{xxx}\right)h_x, \tag{B3}$$

$$N = \left(\frac{1}{2}g\eta^2 + \frac{P^2}{d}\right). \tag{B4}$$

The subscripts x and t denote differentiations with respect to x and t, P is the depth-integrated velocity, d is the total water depth ($d = \eta + h$), the constant B depends on the Boussinesq formulation [*Madsen and Sørensen*, 1993]. Moreover, it is found that $M(\eta)$ may be neglected if the condition $h_x \ll kh$, where $k = k(x)$ is the characteristic local wavenumber, is satisfied.

This is the case in our experiments where $h_x = 0.01$ and $0.64 < kh < 0.81$. Moreover, the correction term $N_{xx}(\eta)$ may be replaced by $N_{xx}(\eta_0)$, where η_0 is the linear approximation of η , that is, satisfying the linear dispersion relation

$$L(\eta_0) = 0. \tag{B5}$$

Finally, the retained first-order nonlinear approximation is

$$L(\eta_1) = N_{xx}(\eta_0). \tag{B6}$$

The first-order nonlinear correction η_1' to the linear approximation $\eta_0 = \eta_{01} + \eta_{02}$ is then given as solution of

$$L(\eta_1') = N_{xx}(\eta_{01} + \eta_{02}) \tag{B7}$$

and the first-order solution is

$$\eta_1 = \eta_0 + \eta_1'. \tag{B8}$$

This is applied in the case where η_{01} is a monochromatic wave

$$\eta_{01} = a\cos(\omega t - \varphi(x)), \tag{B9}$$

where the phase lag is expressed as $\varphi(x) = \int k dx$.

The associated free wave η_{02} is given by

$$\eta_{02} = a_f \cos(2\omega t - \int K dx + \varphi_f), \tag{B10}$$

where both $[\omega, k(x)]$ and $[2\omega, K(x)]$ satisfy the linear dispersion relation, and with $a_f \ll a$, $O(a_f) = a^2/h$.

As a consequence of the quadratic character of N, sum and difference frequency terms expected in the correction η_1' are then ascribed with angular frequency and local wavenumber as follows: $(\omega\ ;\ K-k)$, $(2\omega\ ;\ 2k)$, $(3\omega\ ;\ K+k)$, and $(4\omega\ ;\ 2K)$.

In fact, after some algebra and retaining only the leading order terms $(\omega\ ;\ K-k)$ and $(2\omega\ ;\ 2k)$ in the correction, the first-order nonlinear approximation is finally found as

$$\begin{aligned}\eta(x,t) \;=\; & a\cos(\omega t - \int k dx) \\ & + A_f \cos(\omega t - \int (K-k)dx + \varphi_f) \\ & + a_2 \cos 2(\omega t - \int k dx) \\ & + a_f \cos(2\omega t - \int K dx + \varphi_f),\end{aligned} \tag{B11}$$

with $O(a_2) = a^2/h$, $O(A_f) = a_f a/h \ll a$.

The wave component of circular frequency ω is then the first harmonic of the wave $(\omega\ ;\ k)$ added with the weak first-order correction $(\omega\ ;\ K-k)$ which is the perturbation by the free wave. The wave component of circular frequency 2ω is the sum of the initial free wave and the second harmonic term. Both free wave and second harmonic terms are small in regard to the first harmonic. Moreover, as they propagate at different velocities, they give rise to a beating with local wavenumber $K-2k$. This beating is particularly easy to observe when $a_f \approx a_2$.

Acknowledgments. Financial support to Vincent Rey by the scientific programme PNEC (Programme National d'Environnement Côtier) is acknowledged. The authors are grateful to Stephan Grilli and Richard Van Hooff for a critical reading of the manuscript. The referees of this paper can find here our gratitude for their critical comments and their support of the laboratory studies.

References

Brooke-Benjamin, T., B. Boczar-Karakiewicz, and W. G. Pritchard, Reflection of water waves in a channel with corrugated bed, *J. Fluid Mech., 185*, 249-274, 1987.

Brossard, J., and A. Hémon, Analyse spectrale par effet Doppler de la propagation de la houle, *C. R. Acad. Sci., Ser. II, 320*, 171-176, 1995.

Davies, A. G., The reflection of wave energy by undulations of the seabed, *Dyn. Atmos. Oceans, 6*, 207-232, 1982.

Davies, A. G., and A. D. Heathershaw, Surface-wave propagation over sinusoidally varying topography: Theory and observation, *J. Fluid Mech., 144*, 419-443, 1983.

Dette, H. H., Migration of longshore bars, *Proc. Int. Conf. Coastal Eng.*, 17^{th}, 1476-1492, 1980.

Dulou, C., V. Rey, and M. Belzons, Bar formation on a sloping erodible bed: A laboratory study, *in Proceedings of the*

13th Australasian Fluid Mechanics Conference, vol. 2, pp. 815-818, M.C. Thompson and K. Hourigan, Melbourne, 1998.

Elgar, S., R. T. Guza, B. Raubenheimer, T. H. C. Herbers, and E. L. Gallagher, Spectral evolution of shoaling and breaking waves on a barred beach, *J. Geophys. Res., 102*, 15,797-15,805, 1997.

Flick, R. E., and R. T. Guza, Paddle generated waves in laboratory channels, *J. Waterw., Port Coastal Ocean Div. Am. Soc. Civ. Eng., 106*, 79-97, 1980.

Grue, J., Nonlinear water waves at a submerged obstacle or bottom topography, *J. Fluid Mech., 244*, 455-476, 1992.

Guazzelli, E., V. Rey, and M. Belzons, Higher-order Bragg reflection of gravity surface waves by periodic beds, *J. Fluid Mech., 245*, 301-317, 1992.

Hulsbergen, C. H., Origin, effect and suppression of secondary waves, *Proc. Coastal Eng. Conf.*, 14^{th}, 392-411, 1974.

Kirby, J. T., A general wave equation for waves over rippled bed, *J. Fluid Mech., 162*, 171-186, 1986.

Kirby, J. T., Propagation of surface waves over undulating bed, *Phys. Fluids A, 1*, 1898-1899, 1989.

Lofquist, K. E. B., Sand ripple growth in an oscillary flow water tunnel, *Tech. Pap. 78-5,*, 101 pp., U.S. Army Corps of Eng., 1978.

Madsen, O. S., On the generation of long waves, *J. Geophys. Res., 76*, 8672-8683, 1971.

Madsen, P. A., and O. R. Sørensen, Bound waves and triad interactions in shallow water, *Ocean Eng., 10*(4), 359-388, 1993.

Mei, C. C., Resonant reflection of surface waves by periodic sandbars, *J. Fluid Mech., 152*, 315-335, 1985.

Mei, C. C., T. Hara, and M. Naciri, Note on Bragg scattering of water waves by parallel bars on the seabed, *J. Fluid Mech., 186*, 147-162, 1988.

Miller, M. C., and P. D. Komar, Oscillation sand ripples generated by laboratory apparatus, *J. Sediment. Petrol., 50*, 173-182, 1980.

Nayfeh, A. H., and M. A. Hawwa, Interaction of surface gravity waves on a nonuniformly periodic seabed, *Phys. Fluids, 6*, 209-213, 1994.

Norheim, C. A., T. H. C. Herbers, and S. Elgar, Nonlinear evolution of surface wave spectra on a beach, *J. Phys. Oceanogr., 28*, 1534-1551, 1998.

O'Hare, T. J., and A. G. Davies, A laboratory study of sand bar evolution, *J. Coastal Res., 6*, 531-544, 1990.

O'Hare, T. J., and A. G. Davies, Sand bar formation beneath partially standing waves: Laboratory experiments and model simulations, *Cont. Shelf Res., 13*, 1149-1181, 1993.

Rey, V., Propagation and local behaviour of normally incident gravity waves over varying topography, *Eur. J. Mech. B, 11*(2), 213-232, 1992.

Rey, V., and P. Fraunié, Propagation of surface gravity waves on modulated sloping bottoms, paper presented at XXII EGS General Assembly, Vienna, Austria, April 21-27, 1997.

Rey, V., A. G. Davies, and M. Belzons, On the formation of bars by the action of waves on an erodible bed: A laboratory study, *J. Coastal Res., 11*, 1180-1194, 1995.

Rey, V., E. Guazzelli, and C. C. Mei, Resonant reflection of surface gravity waves by one-dimensional doubly sinusoidal beds, *Phys. Fluids., 8*, 1525-1530, 1996.

Ruessink, B. G., Bound and free infragravity waves in the nearshore zone under breaking and nonbreaking conditions, *J. Geophys. Res., , 103*, 12,795-12,805, 1998.

Saylor, J. H., and E. B. Hands, Properties of longshore bars in the Great Lakes, *Proc. Int. Conf. Coastal Eng.*, 12^{th}, 839-853, 1970.

Scott, T., Sand movement by waves, *Tech. Memo. 48*, 37 pp., Beach Erosion Board, U.S. Army Corps of Engineers, 1954.

Short, A. D., Offshore bars along the Alaskan Arctic coast, *J. Geol., 83*, 209-221, 1975.

Ursell, F., The reflection of waves from a submerged low reef, *rep. N/W/103.41/R5*, Admiralty Res. Lab., 1947.

Yu, J., and C. C. Mei, Formation of sand bars under surface waves, *J. Fluid Mech., in press* 2000a.

Yu, J., and C. C. Mei, Do longshore bars shelter the shore?, *J. Fluid Mech., 404*, 251-268, 2000b.

M. Belzons, and C. Dulou, IUSTI, UMR 6595 du CNRS, Université de Provence, Technopole de Chateau-Gombert, F-13453 Marseille cedex 13, France. belzons@iusti.univ-mrs.fr; dulou@iusti.univ-mrs.fr

V. Rey, Laboratoire de Sondages Electromagnétiques de l'Environnement Terrestre, UPRESA-CNRS 6017, Université de Toulon et du Var, BP 132, F-83957 La Garde Cedex, France. rey@lseet.univ-tln.fr

(Received February 23, 1999; revised March 20, 2000; accepted April 7, 2000.)